Preferred citation: U. Garusinghe, V.S. Raghuwanshi, P. Raj, G. Garnier and W. Batchelor. Investigating silica nanoparticle-polyelectrolyte structures in microfibrillated cellulose films by scattering techniques. In **Advances in Pulp and Paper Research, Oxford 2017**, *Trans. of the XVIth Fund. Res. Symp. Oxford, 2017*, (W. Batchelor and D. Söderberg, eds), pp 823–836, FRC, Manchester, 2018. DOI: 10.15376/frc.2017.2.823.

INVESTIGATING SILICA NANOPARTICLE-POLYELECTROLYTE STRUCTURES IN MICROFIBRILLATED CELLULOSE FILMS BY SCATTERING TECHNIQUES

Uthpala Garusinghe, Vikram Singh Raghuwanshi, Praveena Raj, Gil Garnier and Warren Batchelor*

Bioresource Processing Research Institute of Australia (BioPRIA), Department of Chemical Engineering, Monash University, Clayton 3800, VIC, Australia

ABSTRACT

We report the cationic polyelectrolyte (CPAM)-SiO_2 nanoparticle (NP) interactions in suspension and in a sheet form, when mixed with microfibrillated cellulose (MFC), using dynamic light scattering (DLS) and small angle X-ray scattering (SAXS) techniques. The CPAM-SiO_2 NP suspensions were prepared by adding NPs into CPAM drop wise and composites were prepared by adding CPAM-SiO_2 supension into MFC and through standard paper making procedure. DLS revealed that increase in CPAM dosage creates larger sized CPAM-NP aggregates because more NPs can be picked up by stretched CPAM chains. SAXS study revealed that CPAM-SiO_2 NP assembly in the formed nanopaper fits well with a sperical core shell model (with SiO_2 partially covered with CPAM) and sphere model (SiO_2 alone) combined together. Understanding the interaction between polyelectrolyte-NP system through such scattering techniques enables us to engineer novel cellulose based composites for specfic applications.

* Corresponding author: Gil.garnier@monash.edu

Keywords: Dynamic light scattering (DLS), Small angle X-ray scattering (SAXS), Scanning electron microscopy (SEM), Structure, Polyelectrolyte-nanoparticle system, Cellulose.

1 INTRODUCTION

Nanotechnology involves the manipulation or self-assembly of individual particles or their aggregates into desired configurations, to create materials and devices with new or vastly different properties and functions [1]. Nanoparticles (NPs) take an important role in nanotechnology because of their unique properties and can be selected for their chemical composition, but also can be tailored for their sizes, shape and surface properties [2]. NPs on their own cannot be used as they self-aggregate or pose the danger of uncontrolled release to the environment when dry. Therefore, ideally NPs need to be embedded into a matrix that is strong, flexible, and durable and also allows the surface area of NPs to be readily available.

Using nanocellulose as a supporting matrix combines the advantage of two constituents to give new composite materials with superior properties. Nanocellulose fibres are a new class of material that has received significant attention over the past decade. This material is of technological interest as it is renewable, biodegradable, exhibits excellent mechanical strength and superior barrier properties, while remaining fully compatible with conventional wood fibres [3]. However, embedding NPs into a nanocellulose matrix at times is difficult, especially when both materials are of same charge. In such cases, polyelectrolytes play an important role for the fixation of NPs onto surfaces in charged systems [4].

Polyelectrolytes play an important role in many industrial applications such as wastewater treatment[5], gene and drug delivery[6], [7], flocculation in paper making[5], [8], sensor development [9], [10], mineral processing [5] and coating processes [11]. This is due to their ability to adsorb at solid-liquid interfaces, thus, modifying surface properties and the interactions between particles and their environment [12]. The understanding of the interaction between polyelectrolytes and surfaces are crucial to optimise surface properties for a specific application. Polyelectrolytes and NPs are used in the papermaking industry as they act as retention aids, adhering fines and mineral fillers on the fibre surface [12]–[14], while at the laboratory scale polyelectrolytes have been shown to strongly interact with cellulose nanofibres, lowering the gel-point by bridging between fibres and increasing the flow through the fibre network during filtration [15]. Despite the numerous studies concerning the adsorption of polyelectrolytes onto charged NP surfaces which has been studied in the past using both theoretical [16]–[18] and experimental [4], [11], [12], [19] methods, their modes of action are poorly understood as they depend greatly on the type of polymer and particles in the system

[20]. The conformation of the adsorbed polyelectrolyte on the NP surface is still a largely unexplored subject.

In this paper we quantify the interaction between cationic polyacrylamide – SiO_2 NPs using two complimentary scattering techniques in order to engineer specific structures in the composite. Understanding on the behaviour of cationic dimethylamino-ethyl-methacrylate (CPAM) in SiO_2 nanoparticle (NP) suspension is crucial in production of cellulose-polyelectrolyte-NP based composite films for different applications. Dynamic light scattering (DLS) technique is used to investigate the conformation and changes in hydrodynamic radius of cationic polyacrylamide adsorbed on the surface of SiO_2 NPs. Small angle X-ray scattering (SAXS) technique is used to investigate the effect of CPAM concentration on the SiO_2 NP assemblies formed within the MFC matrix.

2 EXPERIMENTAL METHOD

2.1 Material

Microfibrillated cellulose (MFC) was purchased from DAICEL Chemical Industries Limited, Japan (Grade Celish KY-100G). MFC was supplied at 25 wt% solids contend and stored at 5 °C. MFC has a mean diameter of 73 nm and the aspect ratio of 142 [21]. Cationic dimethylamino-ethyl-methacrylate (CPAM) polymer with molecular weight 13 MDa and charge density 50% was kindly provided by AQUA+TECH, Switzerland from their SnowFlake Cationics range. 22 nm colloidal silica with surface area 220 m^2/g was purchased from Sigma Aldrich at 30 wt% suspension.

2.2 Method

2.2.1 Preparation of MFC, CPAM and silica NP suspensions

A 3 L disintegrator (Mavis Engineering Model No. 8522) was used to disperse 0.2 wt% MFC in deionized water at 15,000 propeller revolutions. 0.01 wt% CPAM suspension was prepared by mixing CPAM with deionized water for minimum of 8 hours prior to the experiments. SiO_2 NPs were diluted to 0.5 wt% from the stock solution using deionized water. The CPAM and SiO_2 NP solutions were sonicated for 2 minutes at 100% amplitude to ensure evenly distribution.

2.2.2 Preparation of pure MFC sheet

Sheets were prepared using a British handsheet maker (model T205) which is equipped with a woven filter with an average opening of 74 microns. 0.2 wt%

pure MFC suspension was poured into the column and allowed water to drain under gravity. When the film was formed, it was taken out using blotting papers and dried at 105 °C using a sheet drier.

2.2.3 Preparation of CPAM-silica NP suspension for DLS

0.5 wt% sonicated SiO_2 NP suspension was added through a peristaltic pump at 10 mL/min into the sonicated 0.01 wt% CPAM solution which was stirred at 200 rpm/min with a magnetic stirrer. Amount of SiO_2 NPs in the suspension was fixed at 0.3 g. The mixing process was repeated for three different surface coverages of CPAM to NPs (0.03, 0.05 and 0.09 mg CPAM/m^2 surface area of SiO_2 NPs). The concentration of the final suspension changes from 0.38–0.26 wt% depending upon CPAM dosage. This method of addition allowed SiO_2 NP suspension to be added drop by drop into the sonicated CPAM solution. Dynamic Light Scattering (DLS) was then used to measure the size of the NPs with adsorbed CPAM on its surface.

2.2.4 Preparation of MFC-CPAM- SiO_2 NP composite for SAXS

Preparation of composite sheets involved mixing MFC (1.2 g at 0.2 wt%), SiO_2 NPs (25 wt% of the total composite at 0.1 wt%) and CPAM (different ratios at 0.01 wt%) suspensions together simultaneously. While SiO_2 NPs and MFC used in composite sheets was fixed, four different CPAM dosages were used (0.07, 0.14, 0.2 and 0.5 mg CPAM/m^2 surface area of SiO_2 NPs). Firstly, CPAM and SiO_2 NP suspensions were mixed together into a beaker through simultaneous addition with two peristaltic pumps. Secondly, CPAM-SiO_2 NP suspension and MFC suspension was mixed again into a beaker through simultaneous addition with two peristaltic pumps to make the final composite suspension. Total mixing time was set to 8 minutes in each step. CPAM was added at different speeds (7.7–55 mL/min) depending on the dosage, SiO_2 was added at 50 mL/min and MFC was added at 75 mL/min. The final concentration of the suspension varied between 0.15–0.11 wt% depending on the CPAM dosage. Final suspension was poured into British handsheet maker for composite processing as mentioned above.

2.3 Characterization

2.3.1 Dynamic light scattering (DLS)

CPAM-SiO_2 NP suspensions prepared above for DLS analysis were used as prepared to measure DLS with a Nanobrook Omni (Brookhaven Instruments) using a cuvette cell at 25 °C. Diameter distribution of the clusters were calculated using the supplied software.

2.3.2 Small angle X-ray scattering (SAXS)

SAXS measurements were conducted at the SAXS/WAXS beamline at the Australian Synchrotron, Melbourne [22]. Measurements were made in a transmission mode with the X-ray energy of 11 keV. Scattered photons were collected at detector distance of 7.2 m using the Pilatus 1 M detector (Dectris, Baden, Switzerland). The isotropic raw detector images were converted to intensity versus q,

$$\left|\vec{q}\right| = q = \frac{4\pi \sin\theta}{\lambda}$$

where θ is the scattering angle and λ is the wavelength (0.113 nm) of incident X-rays. Data reduction with respect to the measurement geometry, masking dead pixels and the beam stop and a subtraction of air scatter were conducted using IDL based ScatterBrain software [23]. The scattered intensity is plotted as a function of the momentum transfer vector q. Data analysis was conducted by fitting the SAXS curves using the SASfit software.

2.3.3 Scanning electron microscopy (SEM)

SEM analysis was performed using FEI Magellan 400 FEGSEM on the composites. Each sample was cut to 3 mm by 3 mm pieces and mounted onto a metal sample holder, coated with a thin layer of Iridium prior to imaging. Accelerating voltage was 3kV and current was 6.3 pA. The images were taken at 30,000× and 100,000× magnifications.

3 RESULTS AND DISCUSSION

3.1 Scanning Electron Microscopy (SEM) of MFC-SiO_2-CPAM composite sheets

Figure 1(a) shows a SEM image of a pure MFC sheet. A wide distribution of pore sizes can be observed. Figure 1(b) shows SEM images of a MFC with 0.5 mg/m^2 CPAM dosage on 22 nm SiO_2 NPs respectively. NPs seem to accommodate themselves to the gaps created by the MFC fibres and fill up without altering the fibre network. While qualitative information can be obtained from SEM, is difficult to fully characterise the samples with SEM alone as (1) SEM images are from a selected area and it does not give enough information about the local distribution of NPs in the matrix, (2) SEM only show the NPs which are on the surface, (3) the interaction or the type of distribution between CPAM-SiO_2 NPs cannot be properly understood or seen. Therefore, SEM alone is not good enough to properly investigate a polyelectrolyte-NP system to optimise performance. Scattering

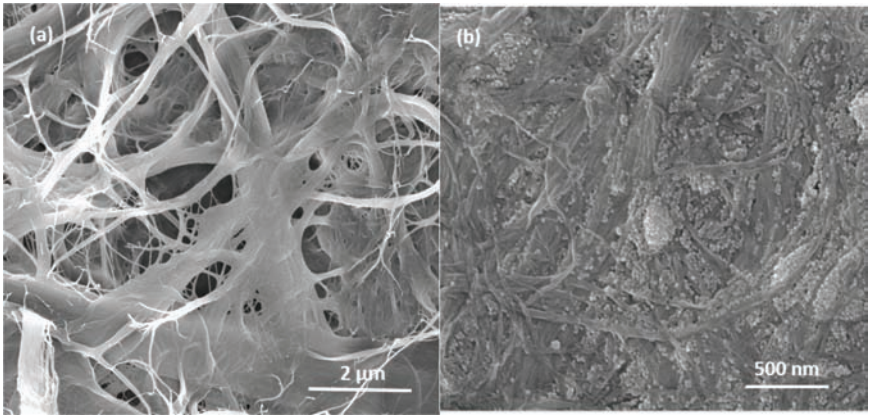

Figure 1. Scanning electron microscopy (SEM) images: (a) pure MFC sheet, and (b) MFC–22 nm SiO_2 NPs–0.5 mg/m^2 CPAM composite at high magnification.

techniques such as DLS and SAXS are useful in obtaining further information on the internal structure of the material in the 1 to 100 nm length scale.

3.2 Dynamic Light Scattering (DLS) on CPAM-NP suspensions

DLS experiments were conducted to reveal the interaction between SiO_2 NPs and CPAM with respect to different dosages of CPAM. Figure 2(a) shows the correlation curves for pure SiO_2 NPs and NPs with two different dosages of CPAM (0.03 mg/m^2 and 0.05 mg/m^2). The correlation curve decays at a slower rate with increase in CPAM dosages. For pure NPs the correlation curve decays at around 200 μsec while for the higher CPAM dosage (0.05 mg/m^2) the correlation curve decays at 3000 μsec. This corresponds to CPAM adsorption onto the SiO_2 NPs which results in formation of aggregates and reduce the diffusion rate of aggregated particles. Distribution of the NPs and NP aggregates obtained from DLS are shown in the Figure 2(b).

The radius of gyration of CPAM with 13 MDa, without accounting for the charged groups is 38 nm when calculated theoretically using the random walk model [24]. Polyelectrolytes with a low charged density have a coiled conformation in solution with smaller diameters which is characterised by a random walk much the same as non-charged polymers in a solvent [25], [26]. Highly charged polymers have stretched out or extended conformations in solution which is due to the closely spaced charged sites resulting in larger diameters [25], [26]. Thus, the actual radius of gyration of CPAM that when stretched out due to repulsion between charged groups on the polymer segment is much larger. In this work, we

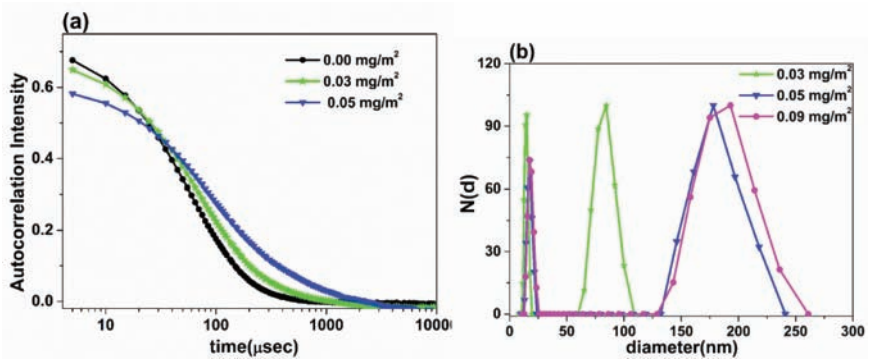

Figure 2. (a) Auto correlation curves of Pure SiO_2 NPs and SiO_2 with CPAM concentration of 0.03 mg/m^2 and 0.05 mg/m^2. (b) Diameter distribution obtained from DLS for SiO_2 NPs with CPAM concentration of 0.03 mg/m^2, 0.05 mg/m^2 and 0.09 mg/m^2.

have used 50% charge density and that is considered fairly high. Therefore, CPAM used in this work is expected to be stretched out and have a more extended conformation on the surface.

Two distinct peaks are seen for each dosage of CPAM in Figure 2(b). There is no significant difference in the diameter with increase in CPAM dosage for Peak 1, which has a maximum in the range 19 nm to 23 nm, consistent with measurements of single particles. However, the intensity of Peak 1 reduces when CPAM dosage increased from 0.05 mg/m^2 onwards, suggesting that number of single SiO_2 NPs that have not formed agglomerates are reducing as the dosage of CPAM increases. With increasing CPAM dosage, the second peak shifted to higher diameters. At 0.003 mg/m^2 (lower dosage), Peak 2 appeared at 85 nm. This peak shifted to 178 nm and 193 nm with 0.05 mg/m^2 and 0.09 mg/m^2 (higher dosages), respectively. This could be due to more stretched out configuration of the polymer causing a high probability of SiO_2 NPs to be picked up and forming larger agglomerates.

However, using DLS as a scattering technique is difficult for higher dosages of CPAM as DLS does not give reliable results when higher amount of polymer is added. At higher doses without a fibre matrix, isolated particles tend to agglomerate into much bigger clusters when compared to being in the sheet form. This is because when CPAM-NP is mixed with MFC to form sheets, fibres has an influence on the size of aggregations and stop bigger agglomerations from forming. Therefore, SAXS is a more suitable scattering technique to measure the particle interactions at higher CPAM dosages.

3.3 Small Angle X-ray Scattering (SAXS) on MFC-NP-CPAM composite sheets

Small Angle X-ray Scattering (SAXS) is a powerful method to give information on the shape, size, distribution of NPs in different kind of matrices [27]–[31]. SAXS experiments were performed to investigate the effect of CPAM on the dispersion of SiO_2 NPs in the MFC fibre matrix. Figure 3(a) shows the SAXS curve from the MFC sheet. No features were observed in SAXS curve which is due to the presence of large structure of MFC fibres with large pore sizes as seen in Figure 1(a). Figure 3(b) shows the fitted SAXS curves for the SiO_2 NPs with different dosages of CPAM (0.07–0.50 mg/m^2: a higher range than the dosages used in DLS).

Further information from the SAXS curves (Figure 3(b)) were extracted by nonlinear fitting using combination of different form factor and structure factor using the software SASfit [32]. The total SAXS scattering intensity can be given as:

$$I_{SAXS}(\vec{q}) = \int_0^\infty N(r)\left|F(q,r,\Delta\eta)\right|^2 S(q,r,\Delta\eta)dr + Bkg + Cq^{-\alpha} \quad (1)$$

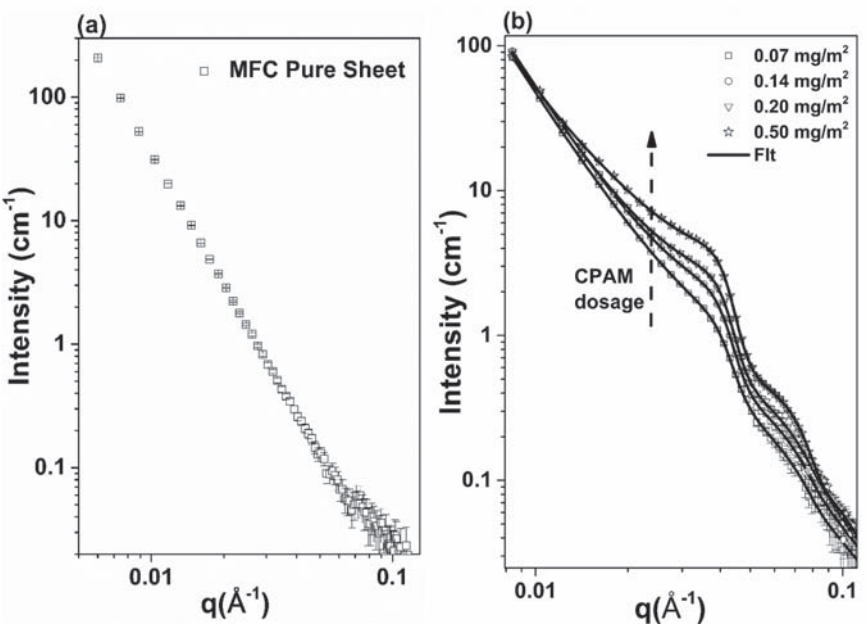

Figure 3. (a) SAXS curve for pure MFC sheet. (b) SAXS curves fitted with the core-shell and sperical models with different CPAM dosages.

Where, $N(r)$ is the particle number distribution, $F(q, r, \Delta\eta)$ is the structure model which contains information about shape and size of the particles. In the structure model, $\Delta\eta$ is the effective electron density difference between the particle and the remaining matrix, q is the transferred momentum, $S(q, r)$ is the structure factor conatins information on the interaction between the particle and *Bkg* is the background with the surface scattering term.

The form factor with the combination of the spherical core shell particle and the spherical particle with the lognormal size distribution fits well for all the scattering curves (Figure 3b). The form factor is defined as:

$$F(q, r, \Delta\eta) = F_{sphere\ shell}(q, r_t, \Delta\eta_s) + F_{sphere}(q, r_t, \Delta\eta_s) \quad (2)$$

where the F_{sphere} is the form factor of sphere as:

$$F_{sphere}(q,r,\Delta\eta) = 3\Delta\eta\frac{\sin qr - qr\cos qr}{(qr)^3} \quad (3)$$

and $F_{sphere\ shell}$ is the form factor for spherical core shell particles and given as:

$$F_{sphere\ shell}(q, r_t, \Delta\eta_s, v, \mu) = F_{sphere}(q, r_t, \Delta\eta_s) - F_{sphere}(q, vr_t, \Delta\eta_s(1-\mu)) \quad (4)$$

where, r_t is the radius of the core (SiO_2) + shell (CPAM), which is related to the core radius as $r = vr_t (0 < v < 1)$, $\Delta\eta_s = \eta_{shell} - \eta_{matrix}$ is the effective electron density difference between shell and matrix and $\mu\Delta\eta_s$ is the effective electron density difference between the core and the matrix. Additionally, the structure factor was included into the fitting procedure [33], [34]. While fitting a SAXS curve, all the structure determining parameters, size distribution parameters, structure factor parameters and the contrast of the particles were free fitting variables.

The obtained parameters show the average SiO_2 particle diameter of 22 ± 3 nm and thickness of the CPAM layer adsorbed onto the SiO_2 NPs is about 5 ± 0.5 nm. The schematic of the electron density profile for the spherical core shell particle is given in the Figure 4(a). It is found that the effective electron density of the core (SiO_2; density 2.4 g/cm^3) is larger than the cellulose matrix ($C_6H_{10}O_5$; density 1.5 g/cm^3). Moreover, the effective electron density of shell (CPAM, density: 1.1 g/cm^3) is smaller than the cellulose matrix.

The evaluated resultant structure factor for the two dosages of CPAM (0.07 mg/m^2 and 0.5 mg/m^2) obtained after fitting the SAXS curve is given in Figure 4(b). There is a small shift in the structure factor peak of high CPAM dosage (0.5 mg/m^2) towards the higher q values with respect to the small CPAM dosage (0.07 mg/m^2). The shift towards higher q values indicates a decrease in the inter-particle distance between the particles with the high dosage of CPAM. However, the

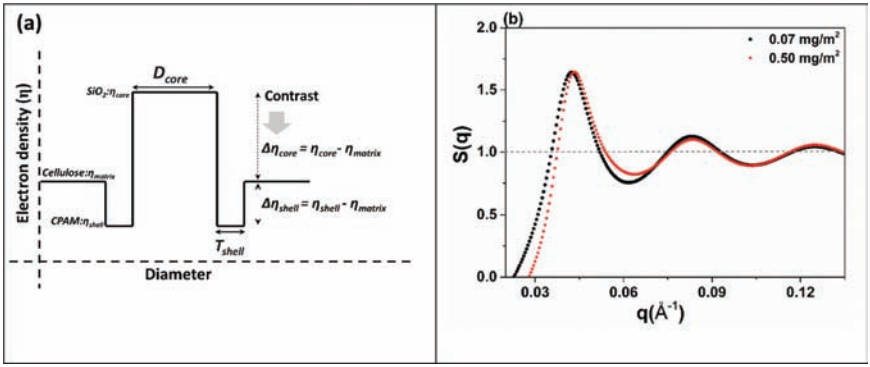

Figure 4. (a) Electron density variation profile for the spherical core shell particle with SiO_2 core, CPAM shell and cellulose matrix, (b) Structure factor obtained after fitting of the SAXS curve for the CPAM dosages of 0.07 mg/m^2 and 0.5 mg/m^2.

difference is not significant and peak sharpness is also almost the same. This result reveals that with increase in CPAM dosage, the interaction between 22 nm SiO_2 NPs does not varies strongly.

Both SiO_2 NPs and MFC are negatively charged and therefore is difficult for SiO_2 to directly adsorb onto/within the cellulose matrix. CPAM is a positively charged polymer with the radius of gyration of 38 nm. CPAM acts as a bridge for SiO_2 NPs to be retained within the cellulose matrix. At low CPAM dosage, the CPAM adsorb onto the SiO_2 NPs surface and spread over the NP surface. It is difficult to identify whether CPAM totally covers the surface of NPs or partially cover the surface. In the case when the CPAM covers the surface of NPs completely, then the CPAM forms a positive shell like region over NPs surface. This will not allow NPs to form aggregates due to the electrostatic repulsion between NPs. In the DLS investigation, it was observed that even at the lowest CPAM dosage the NPs form aggregates. Therefore, it is expected that the CPAM partially covers the NPs surface. This results in distribution of both partly CPAM coated NPs and NPs without any CPAM. SAXS curves fits well with the proposed model of distribution of spherical shell (SiO_2 coated in a layer of CPAM) and sphere model (pure SiO_2). Increase in CPAM dosage results in increasing the number of SiO_2 NP aggregates. However, the interaction within the particles does not vary significantly and remain the same as observed by the variation in structure factor peak (Figure 4(b)).

22 nm SiO2 NP behaves differently with CPAM compared to 8 nm SiO_2 NPs with CPAM which was published previously [14]. This could probably be due to the size difference between SiO_2 NPs. The structure factor reported for 8 nm SiO_2

NPs with increase in CPAM showed that structure factor sharpness increased and the peak shifted towards lower value with respect to low CPAM dosage. This suggests that at low CPAM dosages, loosely bounded NP aggregates in the CPAM chain is formed because of the electrostatic repulsion between NPs, therefore the correlation length of the aggregates were about 25–30 nm in size. At high CPAM dosages, more CPAM is available to neutralize the NPs surface and overcome the electrostatic repulsion between NPs, therefore a strong aggregations between NPs were obtained with a bigger correlation length of about 70 nm [14]. For 22 nm particles used in this study, with increase in CPAM dosages, only the number of structures increases and not the structure size. This proves that different length scales of NPs react differently in a polyelectrolyte system.

We conclude that SAXS technique is a better tool in investigating the polyelectrolyte-NP interactions when the polyelectrolyte concentration is higher. Overall, scattering techniques are essential tools in understanding the behavior of a polyelectrolyte-NP systems to better engineer the properties to develop nanocellulose-NP composites for varies applications.

4 CONCLUSION

Interaction between cationic dimethylamino-ethyl-methacrylate (CPAM) and SiO_2 nanoparticles (NPs) in suspension and in a microfibrillated cellulose (MFC) matrix was investigated using scattering methods. This study is beneficial in understanding a polyelectrolyte-NP system with respect to interactions between them, which cannot be obtained from techniques such as scanning electron microscopy (SEM).

Dynamic light scattering (DLS) shows aggregates of NPs at low dosage of CPAM (0.03 mg/m^2) and aggregate size increased to larger sizes with increase in CPAM dosage further (0.05–0.09 mg/m^2). It was noted that DLS results become unreliable when higher amount of polymer is added as DLS technique is sensitive to charge. Therefore, small angle X-ray (SAXS) techniques as well was used to characterize the system.

SAXS investigation revealed that the distribution of CPAM-NP system fits well with a distribution of spherical shell (from SiO_2 coated in 5 nm layer CPAM around) model and a sphere model (SiO_2 alone) combined, and the number of such systems increase with increase in CPAM dosage. Structure factor obtained from SAXS curves reveals the interaction between NPs does not have a significant effect with respect to the dosage of CPAM.

Overall, this study proves that complimentary scattering techniques are essential in understanding a polyelectrolyte-NP system better to develop nanocellulose based composite material targeted for specific applications.

ACKNOWLEDGEMENT

Thanks to MCEM for scanning electron microscopy. The financial support from Australian research council, Australian paper, Carter Holt Harvey, Circa, Norske Skog, and Visy through the Industry Transformation Research Hub grant IH130100016 is acknowledged. Thanks Monash University for MGS and FEIPRS scholarships. The authors would like to thank to Dr. Tim Ryan, Dr. Nigel Kirby, Dr. Adrian Hawley and Dr. Chris Garvey for assistance during SAXS measurements at SAXS/WAXS beamline in Australian Synchrotron.

REFERENCES

1. B. Farhang. Nanotechnology and lipids. *Lipid Technology* **19**(6):132–135, 2007.
2. K. I. Winey and R. A. Vaia. Polymer nanocomposites. *MRS bulletin* **32**(04):314–322, 2007.
3. J. Kim, S. Yun and Z. Ounaies. Discovery of cellulose as a smart material. *Macromolecules* **39**(12):4202–4206, 2006.
4. L.-E. Enarsson and L. Wågberg. Conformation of preadsorbed polyelectrolyte layers on silica studied by secondary adsorption of colloidal silica. *Journal of Colloid and Interface Science* **325**(1):84–92, 2008.
5. G.M. Moody (ed.). Polymeric flocculants. In *Handbook of Industrial Water Soluble Polymers*, Blackwell Publishing Ltd, pp. 134–173, 2007.
6. M. Dimitrova, Y. Arntz, P. Lavalle, F. Meyer, M. Wolf, C. Schuster, Y. Haïkel, J. C. Voegel and J. Ogier. Adenoviral gene delivery from multilayered polyelectrolyte architectures. *Advanced Functional Materials* **17**(2):233–245, 2007.
7. N. Benkirane-Jessel, P. Schwinté, P. Falvey, R. Darcy, Y. Haïkel, P. Schaaf, J. C. Voegel and J. Ogier. Build-up of polypeptide multilayer coatings with anti-inflammatory properties based on the embedding of piroxicam–cyclodextrin complexes. *Advanced Functional Materials* **14**(2):174–182, 2004.
8. L. Wågberg, L. Winter, L. Ödberg and T. Lindström. On the charge stoichiometry upon adsorption of a cationic polyelectrolyte on cellulosic materials. *Colloids and Surfaces* **27**(4):163–173, 1987.
9. F. Caruso, K. Niikura, D.N. Furlong and Y. Okahata. 1. Ultrathin multilayer polyelectrolyte films on gold: Construction and thickness determination. *Langmuir* **13**(13):3422–3426, 1997.
10. F. Caruso, K. Niikura, D. N. Furlong and Y. Okahata. 2. Assembly of alternating polyelectrolyte and protein multilayer films for immunosensing. *Langmuir* **13**(13):3427–3433, 1997.
11. D. L. Elbert, C. B. Herbert and J. A. Hubbell. Thin polymer layers formed by polyelectrolyte multilayer techniques on biological surfaces. *Langmuir* **15**(16):5355–5362, 1999.
12. S.-C. Liufu, H.-N. Xiao and Y.-P. Li. Adsorption of cationic polyelectrolyte at the solid/liquid interface and dispersion of nanosized silica in water. *Journal of Colloid and Interface Science* **285**(1):33–40, 2005.

13. M. Cadotte, M.-E. Tellier, A. Blanco, E. Fuente, T. G. M. van de Ven and P. Paris. Flocculation, retention and drainage in papermaking: A comparative study of polymeric additives. *Canadian Journal of Chemical Engineering* **85**:240, 2007.
14. U. M. Garusinghe, V. S. Raghuwanshi, C. J. Garvey, S. Varanasi, C. R. Hutchinson, W. Batchelor and G. Garnier. Assembly of Nanoparticles-polyelectrolyte complexes in nanofiber cellulose structures. *Colloids and Surfaces A: Physicochemical and Engineering Aspects* **513**:373–379, 2017.
15. Q. Li, P. Raj, F. A. Husain, S. Varanasi, T. Rainey, G. Garnier and W. Batchelor. Engineering cellulose nanofibre suspensions to control filtration resistance and sheet permeability. *Cellulose* **23**(1):391–402, 2016.
16. F. W. Wiegel. Adsorption of a macromolecule to a charged surface. *Journal of Physics A: Mathematical and General* **10**(2):299, 1977.
17. J.-M. Y. Carrillo and A. V. Dobrynin. Molecular dynamics simulations of polyelectrolyte adsorption. *Langmuir* **23**(5):2472–2482, 2007.
18. M. Turesson, C. Labbez and A. Nonat. Calcium Mediated polyelectrolyte adsorption on like-charged surfaces. *Langmuir* **27**(22):13572–13581, 2011.
19. F. T. Hesselink. On the theory of polyelectrolyte adsorption. *Journal of Colloid and Interface Science* **60**(3):448–466, 1977.
20. J. Gregory and S. Barany. Adsorption and flocculation by polymers and polymer mixtures. *Advances in Colloid and Interface Science* **169**(1):1–12, 2011.
21. S. Varanasi, R. He and W. Batchelor. Estimation of cellulose nanofibre aspect ratio from measurements of fibre suspension gel point. *Cellulose* **20**(4):1885–1896, 2013.
22. N. M. Kirby, S. T. Mudie, A. M. Hawley, D. J. Cookson, H. D. Mertens, N. Cowieson and V. Samardzic-Boban. A low-background-intensity focusing Small-Angle X-Ray Scattering undulator beamline. *Journal of Applied Crystallography* **46**(6):1670–1680, 2013.
23. http://www.synchrotron.org.au/aussyncbeamlines/saxswaxs/software-saxswaxs. SAXS Software ScatterBrain.
24. P. Raj, S. Varanasi, W. Batchelor and G. Garnier. Effect of cationic polyacrylamide on the processing and properties of nanocellulose films. *Journal of Colloid and Interface Science* **447**:113–119, 2015.
25. L. A. Connal, Q. Li, J. F. Quinn, E. Tjipto, F. Caruso and G. G. Qiao. Ph-Responsive poly(acrylic acid) core cross-linked star polymers: Morphology transitions in solution and multilayer thin films. *Macromolecules* **41**(7):2620–2626, 2008.
26. Y. Zhou, G. J. Jameson and G. V. Franks. Influence of polymer charge on the compressive yield stress of silica aggregated with adsorbed cationic polymers. *Colloids and Surfaces A: Physicochemical and Engineering Aspects* **331**(3):183–194, 2008.
27. V. Raghuwanshi, M. Ochmann, F. Polzer, A. Hoell and K. Rademann. Self-assembly of gold nanoparticles on Deep Eutectic Solvent (DES) surfaces. *Chem. Commun.* **50**(63):8693–8696, 2014.
28. V. S. Raghuwanshi, R. Harizanova, D. Tatchev, A. Hoell and C. Rüssel. Structural analysis of Fe–Mn–O nanoparticles in glass ceramics by small angle scattering. *Journal of Solid State Chemistry* **222**:103–110, 2015.
29. V. S. Raghuwanshi, A. Hoell, C. Bocker and C. Rüssel. Experimental evidence of a diffusion barrier around Baf 2 nanocrystals in a silicate glass system by ASAXS. *CrystEngComm* **14**(16):5215–5223, 2012.

30. V. S. Raghuwanshi, C. Russel and A. Hoell. Crystallization of $ZrTiO_4$ nanocrystals in lithium-alumino-silicate glass ceramics: Anomalous Small-Angle X-Ray Scattering investigation. *Crystal Growth & Design* **14**(6):2838–2845, 2014.
31. V. S. Raghuwanshi, D. Tatchev, S. Haas, R. Harizanova, I. Gugov, C. Rüssel and A. Hoell. Structural analysis of magnetic nanocrystals embedded in silicate glasses by anomalous Small-Angle X-Ray Scattering. *Applied Crystallography* **45**(4):644–651, 2012.
32. I. Breßler, J. Kohlbrecher and A. F. Thünemann. SASfit: A tool for Small-Angle Scattering data analysis using a library of analytical expressions. *Journal of Applied Crystallography* **48**(5):1587–1598, 2015.
33. J. B. Hayter and J. Penfold. An analytic structure factor for macroion solutions. *Molecular Physics* **42**(1):109–118, 1981.
34. J.-P. Hansen and J.B. Hayter. A Rescaled Msa Structure Factor for Dilute Charged Colloidal Dispersions. *Molecular Physics* **46**(3):651–656, 1982.

Transcription of Discussion

INVESTIGATING SILICA NANOPARTICLE-POLYELECTROLYTE STRUCTURES IN MICROFIBRILLATED CELLULOSE FILMS BY SCATTERING TECHNIQUES

Uthpala Garusinghe, Vikram Singh Raghuwanshi, Praveena Raj, Gil Garnier and Warren Batchelor

Bioresource Processing Research Institute of Australia (BioPRIA), Department of Chemical Engineering, Monash University, Clayton 3800, VIC, Australia

Roger Gaudreault University of Montreal

First of all, do you know the surface area of the microfibrillated cellulose (MFC) in your system?

Vikram Singh Raghuwanshi Monash University

The surface area of MFC in our composites is about 37 m^2/g of MFC. The surface area of SiO_2 NPs for the 8, 22 and 74 nm particles were 264 m^2, 132 m^2 and 66 m^2, respectively.

Roger Gaudreault

Okay. Did you calculate the surface coverage of the polymer on MFC and the surface coverage of the polymer on the surface of silica nanoparticles (SiO_2-NPs)? This would give you an approximation if you added enough or too much CPAM,

and about the kinetics of interactions between CPAM and SiO_2 as well as CPAM and MFC.

Vikram Singh Raghuwanshi

The evaluated surface coverage of CPAM on nanoparticles is between 0.2 to 0.5 mg/m^2 of nanoparticles.

Roger Gaudreault

Okay, but if we express that in terms of dimensionless theta, do you get half surface coverage or a monolayer, or more than 1 monolayer? Did you validate this?

Vikram Singh Raghuwanshi

We first mixed nanoparticle with the CPAM suspension followed by mixing it with MFC suspension. Therefore, first there is an interaction between nanoparticles and CPAM and then the aggregates of NPs distributed into the MFC network. Experiments are planned to systematically evaluate maximum surface coverage of CPAM over nanoparticles and how free CPAM interacts with the MFC suspension.

Roger Gaudreault

What was the shear rate when you added the CPAM-SiO_2-NPs in the MFC suspension?

Vikram Singh Raghuwanshi

We had used a Breville hand stirrer (power: 600 Watt) with high-turbo mixing. We expect a very high shear rate.